PERGAMON

Available online at www.sciencedirect.com

SCIENCE DIRECT®

Polyhedron 22 (2003) 1727–1733

POLYHEDRON

www.elsevier.com/locate/poly

Exchange bias in Ni_4 single-molecule magnets

En-Che Yang [a], Wolfgang Wernsdorfer [b], Stephen Hill [c], Rachel S. Edwards [c], Motohiro Nakano [a], S. Maccagnano [c], Lev N. Zakharov [d], Arnold L. Rheingold [d], George Christou [e,*], David N. Hendrickson [a,*]

[a] Department of Chemistry and Biochemistry, University of California at San Diego, La Jolla, CA 92093-0358, USA
[b] Laboratoire Louis Néel-CNRS, 25 Avenue des Martyrs, 38042 Grenoble Cedex 9, France
[c] Department of Physics, University of Florida, Gainesville, FL 32611, USA
[d] Department of Chemistry, University of Delaware, Newark, DE 19716, USA
[e] Department of Chemistry, University of Florida, Gainesville, FL 32611-7200, USA

Received 6 October 2002; accepted 12 December 2002

Abstract

The syntheses and physical properties are reported for three single-molecule magnets (SMMs) with the composition $[Ni(hmp)(ROH)Cl]_4$, where R is CH_3 (complex **1**), CH_2CH_3 (complex **2**) or $CH_2CH_2C(CH_3)_3$ (complex **3**) and hmp^- is the monoanion of 2-hydroxymethylpyridine. The core of each complex is a distorted cube formed by four Ni^{II} ions and four alkoxide hmp^- oxygen atoms at alternating corners. Ferromagnetic exchange interactions give a $S = 4$ ground state. Single crystal high-frequency EPR spectra clearly indicate that each of the complexes has a $S = 4$ ground state and that there is negative magnetoanisotropy, where D is negative for the axial zero-field splitting $D\hat{S}_z^2$. Magnetization versus magnetic field measurements made on single crystals with a micro-SQUID magnetometer indicate these Ni_4 complexes are SMMs. Exchange bias is seen in the magnetization hysteresis loops for complexes **1** and **2**.

Keywords: Single-molecule magnets; Nanomagnet; Magnetization tunneling; Superparamagnet; Nickel

1. Introduction

The complex $[Mn_{12}O_{12}(O_2CCH_3)_{16}(H_2O)_4]\cdot 4H_2O\cdot 2CH_3CO_2H$ was found to function as a molecular nanomagnet in 1993 [1,2]. Such a molecule has been called a single-molecule magnet (SMM) [3]. The interest in SMMs has grown considerably since it was found that the reversal of direction of magnetization can occur via quantum mechanical tunneling [4–6]. Steps on magnetization versus magnetic field hysteresis loops and temperature-independent magnetization relaxation rates at low temperatures are two clear indications of quantum tunneling of magnetization (QTM).

Polynuclear manganese complexes with nuclearities ranging from Mn_4 [7–10] to Mn_{30} [11] have been found to function as SMMs. The perchlorate salt of a $[Mn_{18}]^{2+}$ cation has been very recently shown [12] to have the largest spin ($S = 13$) and to be the largest SMM to exhibit QTM. SMMs have been identified that contain Fe [13], V [14] or Ni [15,16].

In this paper we present data for three new Ni_4 SMMs. Preliminary results of micro-SQUID magnetometry and high-frequency electron paramagnetic resonance (HFEPR) measurements on single crystals are presented to characterize these Ni_4 SMMs. An exchange bias is observed in the magnetization hysteresis loops, where the magnetic field at which resonant QTM occurs is shifted from zero-field. Such an exchange bias, due to magnetic exchange interactions between nearby SMMs, was very recently reported [17] for a $[Mn_4]_2$ dimer of $S = 9/2$ SMMs.

* Corresponding authors.
E-mail addresses: christou@chem.ufl.edu (G. Christou), dhendrickson@ucsd.edu (D.N. Hendrickson).

0277-5387/03/$ - see front matter
doi:10.1016/S0277-5387(03)00149-9

2. Experimental

2.1. Syntheses

Crystalline samples of complexes **1**, **2**, and **3** were prepared by similar means. The synthesis of $[Ni(hmp)(CH_2OH)Cl]_4$ is described. $NiCl_2\cdot 6(H_2O)$ (2.37 g, 10 mmol) and hmpH (1.09 g, 10 mmol) were dissolved in 40 ml of methanol, followed by addition of a solution of sodium methoxide (NaOMe 0.54 g, mmol) in 20 ml methanol. The solution was refluxed for a half hour, then slowly cooled down to ambient temperature. Well-shaped crystals suitable for X-ray structure analysis were formed overnight.

2.2. Physical measurements

DC magnetic susceptibility data were collected on powdered microcrystalline samples (restrained in eicosane to prevent torquing) on a Quantum Design SQUID magnetometer equipped with a 5.5 T magnet. A diamagnetic correction was applied to the observed magnetic susceptibilities using Pascal's constants.

High-frequency (40–200 GHz) single crystal EPR measurements were carried out using a millimeter-wave vector network analyzer and a high sensitivity cavity perturbation technique; this instrumentation is described elsewhere [18]. Temperature control in the 2–80 K range was achieved using a variable-flow cryostat. The magnetic field was provided by a superconducting split-pair magnet, which enables angle dependent studies on a single crystal.

Tunneling studies were performed by magnetization measurements on a single crystal using an array of micro-SQUIDs as described in the literature [19].

3. Results and discussion

3.1. Description of structures

X-ray structures were determined for $[Ni(hmp)(MeOH)Cl]_4\cdot H_2O$ (complex **1**) at 173(2) K, $[Ni(hmp)(EtOH)Cl]_4\cdot H_2O$ (complex **2**) at 150(2) K and $[Ni(hmp)(t\text{-BuEtOH})Cl]_4$ (complex **3**) at 218(2) K. The details of these structures will be reported in a later paper [20]. Complexes **1** and **2** crystallize in the space group $I\bar{4}2d$ where the asymmetric unit of both contains two independent $[Ni(hmp)(ROH)Cl]_4$ complexes. Complex **3** crystallizes in the space group $I4_1/a$ where the asymmetric unit contains only one $[Ni(hmp)(t\text{-BuEtOH})Cl]_4$ complex. For all three complexes there is a $[Ni_4(O\text{-hmp})_4]^{4+}$ cubane, and each Ni^{II} ion is six coordinate, being bound to three oxygen atoms of the hmp^- ligand, the nitrogen atom of hmp^-, one Cl^-, and one ROH oxygen atom. There are relatively small differences in the bond distances and angles for the two crystallographically different Ni_4 complexes in both complexes **1** and **2**.

A drawing of the structure of the $[Ni(hmp)(t\text{-BuEtOH})Cl]_4$ molecule in complex **3** is shown in Fig. 1. The molecule has S_4 site symmetry in the crystal, as do the Ni_4 molecules in complexes **1** and **2**. There are no solvate molecules present in the crystal of complex **3**, whereas complexes **1** and **2** each have a H_2O solvate molecule. There is no disorder present in the ligands of complexes **1** and **3**, however the ethyl arm of EtOH ligand in complex **2** is disordered in two positions.

In Fig. 2 is given a stereoview of the packing in the crystal of complex **3**. Each $[Ni(hmp)(t\text{-BuEtOH})Cl]_4$ molecule is surrounded tetrahedrally by four other Ni_4 molecules with a Cl···Cl contact between neighboring Ni_4 molecules of 6.036 Å. Thus, there is a diamond-like lattice of Ni_4 molecules. In the cases of complexes **1** and **2**, each has two inter-penetrating diamond lattices of Ni_4 molecules. For complex **1** the two crystallographically different sublattices of Ni_4 molecules have somewhat different Cl···Cl contact distances of 4.867 and 4.862 Å. In the case of complex **2** the two Cl···Cl contact distances are 4.884 and 4.951 Å. The Cl···Cl contact distances for the EtOH complex are larger than those for the MeOH complex; the *t*-BuEtOH complex has the largest Cl···Cl intermolecular contact distance. In a simple sense, as the steric bulk of the ROH ligand is increased, there is an increase in the separation between Ni_4 molecules and, consequently, an increase in the intermolecular Cl···Cl contact distances.

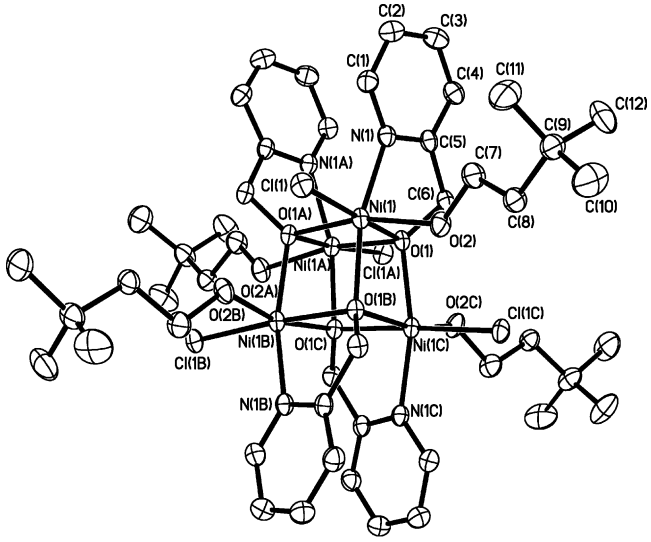

Fig. 1. ORTEP representation of $[Ni(hmp)(t\text{-BuEtOH})Cl]_4$ showing 50% probability ellipsoids.

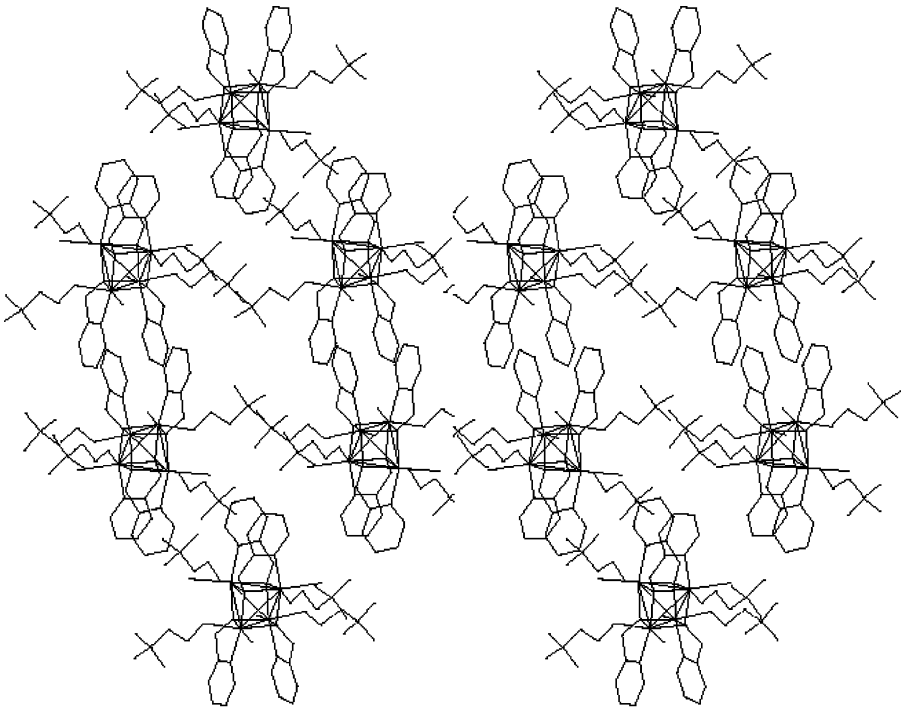

Fig. 2. Stereoview of the packing in the crystal of [Ni(hmp)(*t*-BuEtOH)Cl]$_4$. Only the ligand atoms bonded directly to the Ni atoms are shown for clarity.

3.2. DC magnetic susceptibility studies

Variable-temperature magnetic susceptibility measurements were performed on powder samples of **1**, **2**, and **3** between 300 and 1.8 K. Fig. 3 gives a plot of $\chi_M T$ versus temperature for complex **3**; similar data were measured for the other two complexes. It can be seen that as the temperature is decreased from 300 to $\sim$10 K there is an increase in $\chi_M T$ (equivalent to μ_{eff}^2 for an insolated complex) and below $\sim$10 K there is a decrease in $\chi_M T$. These data are similar to those found [21] for [Ni(OMe)(dbm)(MeOH)]$_4$, which has a $S = 4$ ground state. That is, the spin only value of $\chi_M T$ for a $S = 4$ molecule with $g = 2.0$ is 10 cm^3 K mol^{-1}, which is close to the maximum value found for complex **3** at $\sim$10 K. Magnetic susceptibility data have been reported [21–26] for several Ni_4 cubane complexes. Since the Ni_4 molecule in complex **3** has S_4 site symmetry, it would be expected that all Ni$\cdots$Ni magnetic exchange interactions in the Ni_4 molecule would be equivalent and this gives the spin Hamiltonian in Eq. (1):

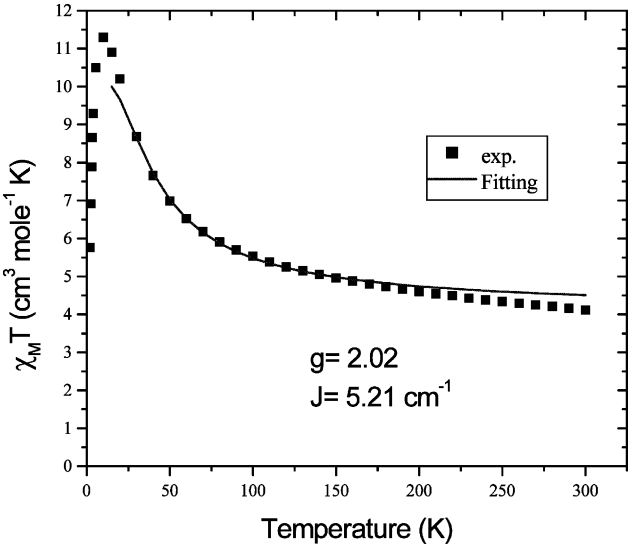

Fig. 3. Plot of $\chi_M T$ versus temperature for a powder sample of [Ni(hmp)(*t*-BuEtOH)Cl]$_4$, where χ_M is the molar paramagnetic susceptibility. The solid line represents a least-squares fit of the data in the region 15–300 K to the Van Vleck equation (see text).

$$\hat{H} = -2J(\hat{S}_1\cdot\hat{S}_2 + \hat{S}_1\cdot\hat{S}_3 + \hat{S}_1\cdot\hat{S}_4 + \hat{S}_2\cdot\hat{S}_3 + \hat{S}_2\cdot\hat{S}_4 + \hat{S}_3\cdot\hat{S}_4) \quad (1)$$

The Kambe equivalent operator technique gives directly an expression (Eq. (2)) for the energies of the 19 different spin states of a Ni_4 as:

$$E(S_T) = -J[S_T(S_T+1)] \quad (2)$$

where $\hat{S}_T = \hat{S}_1 + \hat{S}_2 + \hat{S}_3 + \hat{S}_4$ to give S_T values of 4, 3, 2, 1, and 0. Substitution of the energies and degeneracies of these 19 spin states into the Van Vleck equation gives a simple theoretical expression for the molar susceptibility of a symmetric Ni_4^{II} molecule. The data for complex **3** were least-squares fit to this expression to give $J = +5.2$ cm^{-1} and $g = 2.02$. Thus, in complex **3** there are ferromagnetic interactions between the Ni^{II} ions to give a $S = 4$ ground state. The same conclusion can be

made for complexes **1** and **2**. Single-ion zero-field interactions need to be included in this analysis, but this will be detailed in a later paper [20].

The nature of the ground state of the Ni_4 molecules in complexes **1**, **2**, and **3** can be best probed by studying the magnetization of each complex in the 2.0–4.0 K range in magnetic fields of 1.0, 2.0, 3.0, 4.0 and 5.0 T. In Fig. 4 is given a plot of the reduced magnetization ($M/N\mu_B$) versus H/T for a polycrystalline sample of complex **3**. A full matrix diagonalization (powder average) of the spin Hamiltonian matrix for a $S=4$ state experiencing a Zeeman interaction and both an axial zero-field interaction ($D\hat{S}_z^2$) as well as the quartic zero-field interaction $B_4^0\hat{O}_4^0$ permitted by the symmetry of the complex **3** gives the solid lines shown in Fig. 4. There is a good least-squares fit of the data to give $g=2.16$, $D=-0.61$ $cm^{-1}=-0.88$ K and $B_4^0=-2.8\times10^{-5}$ $cm^{-1}=-4.9\times10^{-5}$ K. The data for complex **2** gives $g=2.12$, $D=-0.60$ $cm^{-1}=-0.86$ K and $B_4^0=-4.5\times10^{-5}$ $cm^{-1}=-6.5\times10^{-5}$ K and for complex **1** $g=2.09$, $D=-0.60$ $cm^{-1}=-0.87$ K and $B_4^0=-4.6\times10^{-5}$ $cm^{-1}=-6.6\times10^{-5}$ K.

3.3. High-frequency EPR data

Single crystal HFEPR data were collected for complexes **1**, **2**, and **3**. Frequencies in the range of 40–200 GHz were employed to probe the ground states of these Ni_4 complexes. The results of a preliminary analysis of these data are presented here. The HFEPR data definitively confirm that these Ni_4 complexes have a $S=4$ ground state and that the axial zero-field splitting parameter D is negative.

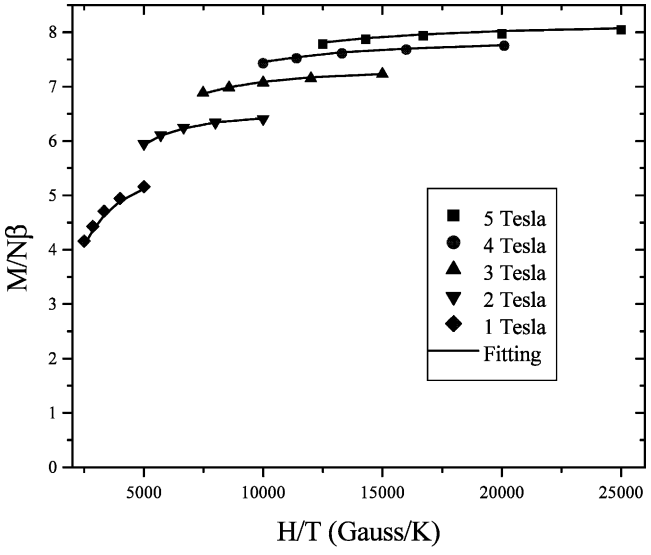

Fig. 4. Plot of reduced magnetization, $M/N\mu_B$ where M is magnetization, N is Avogadro's number and μ_B is the Bohr magneton, versus H/T. Data were collected at magnetic fields of 1.0, 2.0, 3.0, 4.0 and 5.0 T. The solid lines represent a least-squares fit, involving a full matrix diagonalization and a powder average.

The temperature dependence of the HFEPR spectrum for complex **3** is illustrated in Fig. 5. A single crystal was oriented so that the magnetic field is parallel to the easy axis of magnetization for the Ni_4 molecules. Fine structure transitions are seen that correspond to the $m_s=-4$ to $m_s=-3$, $m_s=-3$ to $m_s=-2$, etc., transitions. When the temperature of the crystal is decreased, the transitions at the lowest field become the most intense. This indicates that the axial zero-field splitting parameter D in the $D\hat{S}_z^2$ spin Hamiltonian operator is negative. Similar observations were also made for complexes **1** and **2**. This shows that these three Ni_4 complexes have negative magnetoanisotropy, as required for a molecule to be a SMM.

Single crystal HFEPR spectra were run for all three Ni_4 complexes. Fig. 6 shows the 10 K spectra obtained at approximately 190 GHz, where the magnetic field is parallel to the easy axis of each crystal. The data obtained for the *t*-BuEtOH complex **3** are the easiest to interpret. A series of more-or-less evenly spaced double peaks is observed, with the intensity decreasing for successive pairs of peaks. Speculation as to the origin of the splitting is given below. Separate fits to the $S=4$ Hamiltonian (Eq. (3)) for the lower (L) and upper (U) split peaks were carried out with data taken at eight different frequencies. The two fits are quite good and give for the L peaks $D=-0.600$ cm^{-1}, $B_4^0=-1.2\times10^{-4}$ cm^{-1} and $g_z=2.3$, whereas for the U peaks $D=-0.577$ cm^{-1}, $B_4^0=-1.2\times10^{-4}$ cm^{-1} and $g_z=2.3$.

$$\hat{H}=g_z\mu_B\hat{B}_z\cdot\hat{S}_z+D\hat{S}_z^2+B_4^0\hat{O}_4^0 \tag{3}$$

The HFEPR spectra for the MeOH and EtOH complexes show much broader absorptions and much larger splittings in the fine structure than seen for the *t*-BuEtOH complex. Temperature dependencies and fits to Eq. (3) led to the assignments of peaks that is indicated in Fig. 6. Thus, the MeOH complex **1** shows the largest splitting (L and U peaks) in the $m_s=-4$ to

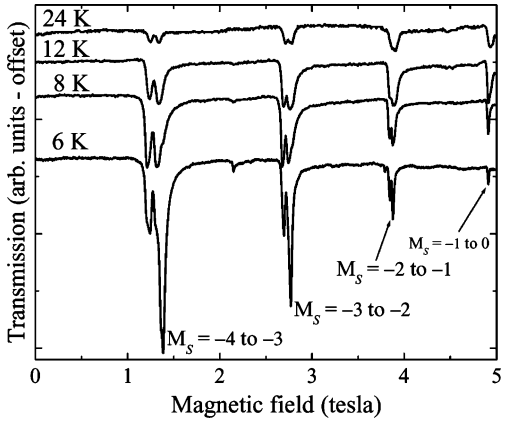

Fig. 5. HFEPR spectra run at 173 GHz for a single crystal of $[Ni(hmp)(t\text{-BuEtOH})Cl]_4$. The magnetic field is oriented parallel to the easy axis of magnetization of the crystal.

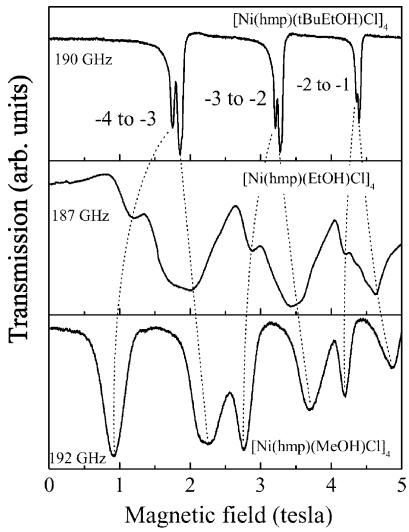

Fig. 6. A comparison of the nominally 190 GHz HFEPR spectra for single crystals maintained at 10 K. In each case the magnetic field is parallel to the easy axis of the crystal. The dashed lines indicate how the splittings of fine structure peaks vary from one Ni_4 complex to another.

$m_s = -3$ fine structure, and the *t*-BuEtOH complex **3** the smallest splitting. Fitting of the data for complexes **1** and **2** give the parameters: $D_L = -0.72\ cm^{-1}$, $D_U = -0.50\ cm^{-1}$, $B_4^0 = -2 \times 10^{-4}\ cm^{-1}$ and $g_z = 2.2$ for complex **1**; $D_L = -0.67\ cm^{-1}$, $D_U = -0.61\ cm^{-1}$, $B_4^0 = -1.2 \times 10^{-4}\ cm^{-1}$ and $g_z = 2.2$ for complex **2**.

Additional experiments have to be carried out to understand the origin of the splittings of the fine structure seen for these Ni_4 SMMs. Basically, there are two possible types of origins: (1) different environments about Ni_4 molecules in the crystal; and (2) intermolecular magnetic exchange interactions between Ni_4 molecules in the crystal. Complexes **1** and **2** do each have, in fact, two crystallographically different Ni_4 molecules. On the other hand, complex **3** only has one Ni_4 molecule in its asymmetric unit. Multiplicities of peaks may be due to different local 'environments' for Ni_4 molecules in a crystal. In addition to crystallographically different Ni_4 molecules, there are other possible differences between Ni_4 molecules. In the case of complexes **1** and **2** there are H_2O solvate molecules. Depending on how these H_2O solvate molecules are arranged about Ni_4 molecules and whether some of these H_2O molecules are absent, Ni_4 molecules that are different may be present. The hmp^- ligand chelates a Ni^{II} ion to form a five-membered ring. This ring could have different conformations that freeze out at the low temperatures in the crystal. Since there are four hmp^- ligands, differences in Ni_4 molecular environments may arise from different hmp^- ligand conformations. In the case of the EtOH complex, the EtOH ligand exhibits a disorder between two positions.

It is also possible the splitting observed for fine structure peaks is attributable to intermolecular magnetic exchange interactions. As described above, each of the complexes **1**, **2** and **3** consist of a diamond-like lattice of Ni_4 molecules. The four Cl^- ligands associated with a Ni_4 molecule are involved in Cl···Cl contacts with four neighboring Ni_4 molecules. The Cl···Cl contact distances (4.862 and 4.867 Å) are the shortest for the MeOH complex, of intermediate value (4.884 and 4.951 Å) for the EtOH complex, and are the largest (6.036 Å) for the *t*-BuEtOH. This logically follows the relative steric bulk of the three ROH ligands.

3.4. Magnetization hysteresis loops

An array of micro-SQUIDs was employed to determine how the magnetization of a single crystal responds to an external magnetic field [19]. Magnetization versus field data were collected in the range of 0.040–6.0 K and at scan rates of 0.002–0.56 T s^{-1}. Figs. 7–9 show typical data for the three Ni_4 complexes. The observed time and temperature dependent hysteresis suggest that complexes **1**, **2** and **3** are SMMs. However, the hysteresis loops of complexes **1** and **2** show appreciable exchange bias effects. We therefore call them exchange biased SMMs. For all three samples, the relaxation rates are temperature-independent below 0.2 K suggesting ground state tunneling.

Fig. 7 illustrates the magnetization hysteresis response of a single crystal of the MeOH complex **1** measured at 0.040 K and at two scan rates. The external magnetic field is applied parallel to the easy axis of magnetization. In the crystals of these Ni_4 SMMs all of the molecules are oriented so that their easy axes are parallel, Fig. 2. For the MeOH complex, after saturation in a 1.4 T negative field, the field is swept towards zero. The first step is observed at −0.72 T, followed by two other steps at −0.33 T and −0.19 T where the rate of decrease of

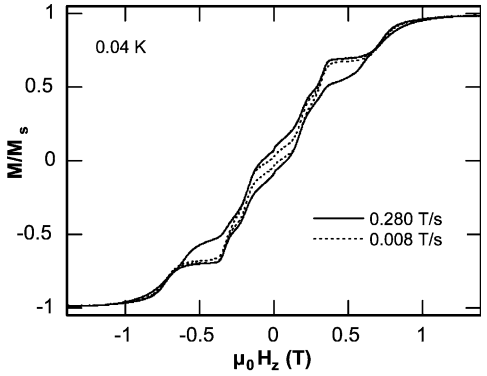

Fig. 7. Magnetization (M) of a single crystal of $[Ni(hmp)(MeOH)Cl]_4 \cdot H_2O$ (plotted as a fraction of maximum value of M_s) versus applied magnetic field ($\mu_o H$). The magnetic field is parallel to the easy axis. The magnetization loops were run at 0.040 K at two different scan rates.

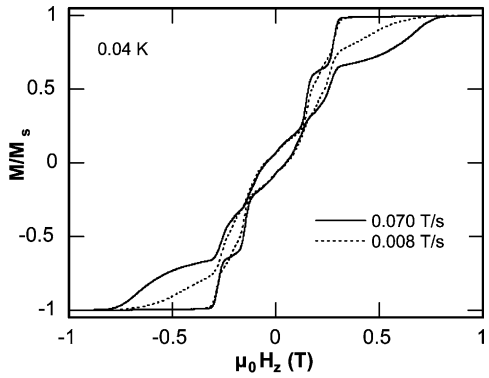

Fig. 8. Magnetization (M) of a single crystal of [Ni(hmp)(EtOH)Cl]$_4$·H$_2$O (plotted as a fraction of maximum value of M_s) versus applied magnetic field ($\mu_o H$). The magnetic field is parallel to the easy axis. The magnetization loops were run at 0.040 K at two different scan rates.

magnetization increases due to a resonant tunneling of the direction of magnetization. For most SMMs the first resonant tunneling step is observed at zero-field. There is clearly an exchange bias present for complex **1** affecting the field at which magnetization tunneling occurs.

The first SMM that has been reported [17] to exhibit such an exchange bias is $[Mn_4O_3Cl_4(O_2CEt)_3(py)_3]_2$. This complex crystallizes in the $R\bar{3}$ space group with pairs of $S = 9/2$ Mn_4 molecules lying 'head-to-head'. The $[Mn_4]_2$ dimer is held together by six C–H···Cl hydrogen bonds and one Cl···Cl interaction. The supramolecular linkage within the $[Mn_4]_2$ dimer leads to a weak antiferromagnetic exchange interaction ($J = -0.05$ K for $\hat{H} = -2J\hat{S}_1 \cdot \hat{S}_2$) between the two $S = 9/2$ SMMs. The hysteresis loops for non-interacting $S = 9/2$ Mn_4 SMMs show their first step at zero-field. The first step is seen at -0.33 T for the $[Mn_4]_2$ dimer. The weak antiferromagnetic interaction between the two $S = 9/2$ SMMs in this dimer shifts the first hysteresis step to -0.33 T.

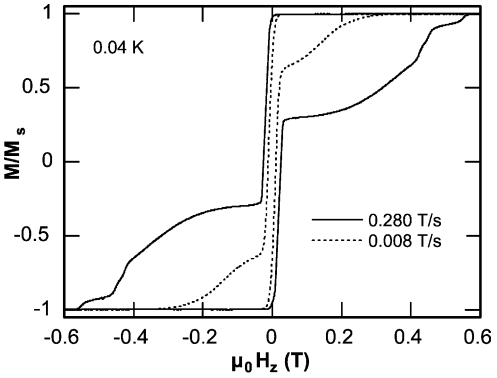

Fig. 9. Magnetization (M) of a single crystal of [Ni(hmp)(t-BuEtOH)Cl]$_4$ (plotted as a fraction of maximum value of M_s) versus applied magnetic field ($\mu_o H$). The magnetic field is parallel to the easy axis. The magnetization loops were run at 0.040 K at two different scan rates.

In the case of Ni_4 complex **1** there are probably intermolecular antiferromagnetic exchange interactions between Ni_4 molecules as a result of the Cl···Cl contacts. Each Ni_4 molecule is exchange coupled to its four nearest neighbor Ni_4 molecules. Because the exchange path are not all identical and of different strength, the diamond-like 3-dimensional exchange interacting lattice leads to three exchange bias steps.

Based on the longer Cl···Cl contact distances present for the EtOH complex **2**, it would be reasonable to expect that the exchange bias for this complex would be less than seen for the MeOH complex **1**. Such is the case, as can be seen from the hysteresis loops plotted for complex **2** in Fig. 8. After saturation in a negative magnetic field, sweeping the magnetic field toward zero gives the first step at -0.28 and -0.15 T. The exchange bias is clearly smaller for the EtOH complex than for the MeOH complex.

Since the t-BuEtOH complex has the largest Cl···Cl contact distance of the three complexes, it would be expected to exhibit the weakest intermolecular antiferromagnetic exchange interaction between neighboring Ni_4 molecules. As a consequence, it would be expected that, in the series of three Ni_4 SMMs, the t-BuEtOH complex would have the smallest exchange bias in its magnetization hysteresis loop. Fig. 9 confirms that this is the case. In fact, the exchange bias in the t-BuEtOH complex is negligible as indicated by the fact that the first step occurs essentially at zero-field. This first step is quite sharp, indicating that there is a relatively large rate of magnetization tunneling.

It is interesting to note that the t-BuEtOH complex not only shows a negligible exchange bias, but this complex exhibits HFEPR absorptions that are considerably narrower than observed for the other two complexes. It is tempting to attribute the fine structure splitting seen in the HFEPR spectra to intermolecular exchange interactions, for the magnitude of the splitting parallels the exchange bias seen in the magnetization hysteresis loops. Further experiments and a theoretical analysis are needed to establish this.

Finally, it is important to comment on the small coercive fields seen in the magnetization hysteresis loops, Figs. 7–9. Magnetization relaxation decay data have been measured for these three Ni_4 SMMs. The relaxation rate at resonance steps is very fast (between ms and s) whereas it can be several 100s outsite the resonance steps. It is clear that the quantum tunneling of the direction of magnetization occurs at a rate that is fast compared to previously studied SMMs. This reflects the large transverse zero-field interactions that must be present in these Ni_4 complexes.

Each Ni^{II} is six coordinate with an O_4NCl ligation. Single-ion axial zero-field splitting ($D\hat{S}_z^2$) for a six coordinate O_6 Ni^{II} can be such that D is positive and ranges up to several cm^{-1} in magnitude [27]. If the

single-ion zero-field interaction at each Ni^{II} ion in complexes **1**, **2** and **3** is characterized by a large positive D-value, then the negative D-value for the Ni_4 complexes could be the result of having the single-ion D-tensors oriented perpendicular to the easy axis of each Ni_4 SMM. This would also have the effect of giving relatively large transverse zero-field interactions for the Ni_4 molecules. Rapid magnetization tunneling would result.

4. Conclusion

Three molecules with the composition $[Ni(hmp)(ROH)Cl]_4$, where $R = CH_3$ for complex **1**, $R = Et$ for complex **2** and $R = t$-BuEtOH for complex **3**, have been shown to be SMMs. Step-structured magnetization versus magnetic field hysteresis loops were observed. In the cases of complexes **1** and **2** an appreciable exchange bias is evident in the hysteresis loops. The first step is shifted considerably from zero-field by virtue of intermolecular antiferromagnetic exchange interactions between Ni_4 complexes in the crystals. Quite interesting HFEPR spectra have been obtained for single crystals.

5. Supplementary material

Crystallographic data for the structural analysis have been deposited with the Cambridge Crystallographic Data Centre, CCDC No. 195520, 195521 and 195522. Copies of this information may be obtained free of charge from The Director, CCDC, 12 Union Road, Cambridge, CB2 1EZ, UK (fax: +44-1223-336033; e-mail: deposit@ccdc.cam.ac.uk or www: http://www.ccdc.cam.ac.uk).

Acknowledgements

This work was supported by the National Science Foundation.

References

[1] R. Sessoli, D. Gatteschi, A. Caneschi, M. Novak, Nature 365 (1993) 149.
[2] R. Sessoli, H.-L. Tsai, A.R. Schake, S. Wang, J.B. Vincent, K. Folting, D. Gatteschi, G. Christou, D.N. Hendrickson, J. Am. Chem. Soc. 115 (1993) 1804.
[3] S.M.J. Aubin, M.W. Wemple, D.M. Adams, H.-L. Tsai, G. Christou, D.N. Hendrickson, J. Am. Chem. Soc. 118 (1996) 7746.
[4] J.R. Friedman, M.P. Sarachik, J. Tejada, J. Maciejewski, R. Ziolo, J. Appl. Phys. 79 (1996) 6031.
[5] J.R. Friedman, M.P. Sarachik, J. Tejada, R. Ziolo, Phys. Rev. Lett. 76 (1996) 3830.
[6] L. Thomas, F. Lionti, F.R. Ballou, D. Gatteschi, R. Sessoli, B. Barbara, Nature 383 (1996) 145.
[7] N. Aliaga, K. Folting, D.N. Hendrickson, G. Christou, Polyhedron 20 (2001) 1273.
[8] S.M.J. Aubin, N.R. Dilley, L. Pardi, J. Krzystek, M.W. Wemple, L.-C. Brunel, M.B. Maple, G. Christou, D.N. Hendrickson, J. Am. Chem. Soc. 120 (1998) 4991.
[9] S.M.J. Aubin, M.W. Wemple, D.M. Adams, H.-L. Tsai, G. Christou, D.N. Hendrickson, J. Am. Chem. Soc. 118 (1996) 7746.
[10] S. Wang, M.S. Wemple, J. Yoo, K. Folting, J.C. Huffman, K.S. Hagen, D.N. Hendrickson, G. Christou, Inorg. Chem. 39 (2000) 1501.
[11] M. Soler, E. Rumberger, K. Folting, D.N. Hendrickson, G. Christou, Polyhedron 20 (2001) 1365.
[12] E.K. Brechin, C. Boskovic, W. Wernsdorfer, J. Yoo, A. Yamaguchi, E.C. Sañudo, T.R. Concolino, A.L. Rheingold, H. Ishimoto, D.N. Hendrickson, G. Christou, J. Am. Chem. Soc. 124 (2002) 9710.
[13] A. Caneschi, D. Gatteschi, C. Sangregorio, R. Sessoli, L. Sorace, A. Cornia, M.A. Novak, C. Paulsen, W. Wernsdorfer, J. Magn. Magn. Mater. 200 (1999) 182.
[14] S.L. Castro, Z. Sun, C.M. Grant, J.C. Bollinger, D.N. Hendrickson, G. Christou, J. Am. Chem. Soc. 120 (1998) 2365.
[15] M. Nakano, G.-E. Matsubayashi, T. Muramatsu, T. Kobayashi, K. Amaya, J. Yoo, G. Christou, D.N. Hendrickson, Mol. Cryst. Liq. Cryst. 376 (2002) 405.
[16] C. Cadiou, M. Murrie, C. Paulsen, V. Villar, W. Wernsdorfer, R.E.P. Winpenny, Chem. Commun. (2001) 2666.
[17] W. Wernsdorfer, N. Aliaga-Alcade, D.N. Hendrickson, G. Christou, Nature 416 (2002) 406.
[18] M. Mola, S. Hill, P. Goy, M. Gross, Rev. Sci. Instrum. 71 (2000) 186.
[19] W. Wernsdorfer, Adv. Chem. Phys. 118 (2001) 99.
[20] E.-C. Yang, W. Wernsdorfer, S.O. Hill, R.S. Edwards, M. Nakano, S. Maccagnano, L.N. Zakharov, A.L. Rheingold, G. Christou, D.N. Hendrickson, Polyhedron 22 (2003) doi: 10.1016/S0277-5387(03)001736.
[21] M.A. Halcrow, J.-S. Sun, J.C. Huffman, G. Christou, Inorg. Chem. 34 (1995) 4167.
[22] J.A. Barnes, W.E. Hatfield, Inorg. Chem. 10 (1971) 2355.
[23] P.D.W. Boyd, R.L. Martin, G. Schwarzenbach, Aust. J. Chem. 41 (1988) 1449.
[24] W.L. Gladfelter, M.W. Lynch, W.P. Schaefer, D.N. Hendrickson, H.B. Gray, Inorg. Chem. 20 (1981) 2390.
[25] L. Ballester, E. Coronado, A. Gutiérrez, A. Monge, M.F. Perpiñán, E. Pinilla, T.C. Rico, Inorg. Chem. 31 (1992) 2053.
[26] A. Escuer, M. Font-Bardía, S.B. Kumar, X. Solans, R. Vicente, Polyhedron 18 (1999) 909.
[27] A. Bencini, E. Berti, A. Caneschi, D. Gatteschi, E. Giannasi, I. Invernizzi, Chem. Eur. J. 8 (2002) 3660.